Flow inside Micro-Channel Bounded by Superhydrophobic Surface with Eccentric Micro-Grooves

Yu Chen, Weiwei Ren, Xiaojing Mu, Feng Zhang, Yi Xu

***Abstract*—**The superhydrophobic surface is widely used to reduce friction for the flow inside micro-channel and can be used to control/manipulate fluid, cells and even proteins in lab-on-chip. Fabricating micro grooves on hydrophobic surfaces is a common method to obtain such superhydrophobic surface. This study utilized the numerical method to investigate the effect of eccentric micro-grooves on the friction of flow inside micro-channel. A detailed parametric study was conducted to reveal how the eccentricity of micro-grooves affects the micro-channel flow under different grooves sizes, channel heights, Reynolds number. The results showed that the superhydrophobic surface with eccentric micro-grooves induces less friction than the counter part with aligning micro-grooves, which means requiring less power for pumps.

***Keywords*—**Superhydrophobic, transverse grooves, heat transfer, slip length, microfluidics.

I. Introduction

THE physical dimension of micron-channel is reduced to accommodate more channels invariably such as in lab-on-chip applications, leading to larger driving pressure needed to maintain the flow throughout to overcome the increased skin friction. It is a challenge to ensure such a high value of pressure for the micron-scale system, where elasticity (i.e., compressibility) of the liquid has to be considered, which can take minutes or even longer to compress liquid in the chamber [1]. This motivates the utilization of other forms of driving force (such as electrical force, magnetic forces and Lorentz forces) and/or the search for drag reduction means to keep the pressure to a manageable level [1]. It is a common belief since the beginning of the modern fluid mechanics that the drag on a smooth surface is always lower than that on a rough surface [2]-[5]. This is actually not the case as documented through the development of special drag reducing surface topographies see recent reviews in [6]).

When the size of (micro) fluid system shrinks, surface forces such as capillary force become dominant. As such, it can be used as the driving force and employed to overcome skin friction by the so-called super-hydrophobic effect [7]. This is combining the effect of hydrophobicity of the liquid w.r.t. surface material and surface topography, with the research being inspired by the unique water-repellent properties of the lotus leaf [8]. When a super-hydrophobic surface is submerged inside a liquid, gas bubbles which are trapped in microstructures (grooves, post/pillars and pores/holes) on the solid substrate surface can effectively reduce the shear stress experienced by the liquid, as the shear between the liquid and solid is replaced by the shear between the liquid and gas.

The overall effect of super-hydrophobic surface on the flow is that the original no-slip boundary condition is transformed into slip boundary condition, and the slip velocity is proportional to the shear rate at the wall

$$u|_w = \lambda \left.\frac{\partial u}{\partial y}\right|_w$$

where λ is the slip length [9], [10]. For micro-fluidic or nano-fluidic devices with super-hydrophobic surface whose characteristic length scale L_c and slip length λ are both in the order of micrometers [11], [12], slip has a significant effect on the flow and drag due to the large Knudsen number $Kn = \lambda/L_c$ [13]-[15]. Thus, much works have been focused on the means to increase the slip length of super-hydrophobic surface, such as increasing hydrophobicity through changes in surface chemistry [16]-[20] and correctly shaping the surface pores/roughness [21]. Normally, the configuration of roughness on the surface influences the overall drag reduction significantly, where longitudinal microgrooves are believed to induce the greatest drag reduction [22]-[25]. It is shown that the drag reduction and effective slip length becomes greater for higher shear-free fraction and the reduced relative channel hydraulic diameter [12], [26]. Davies et al. [26] found that the effective slip length is closely correlated to the local streamwise velocity profile and interfacial velocity, where higher interfacial velocity indicates greater drag reduction and thus higher slip length. At higher Reynolds number, less drag reduction is reported for laminar flow [27], [28].

On further work, besides focusing on the surface roughness shape, the effective slip length is found to be sensitive on the curvature to the water-air interface, which has been reported in experimental [29], analytical [30], [31] and computational studies [29], [32]-[34]. In addition, Kashaninejad et al. [35] pointed out that microhole eccentricity affects the drag reduction efficiency of microchannel with super-hydrophobic surface, which is correlated to the contact angle hysteresis. Generally, microchannels with super-hydrophobic surface on both walls induces greater drag reduction and effective slip

Y. Chen is with the Institute of High Performance Computing, 1 Fusionopolis Way, #16-16 Connexis North, Singapore 138632 (e-mail: yuchen1986sg@gmail.com).

W. Ren is with DHI Water & Environment (S) Pte Ltd, 1 Cleantech Loop, #03-05 CleanTech One, Singapore 637141.

Y. Chen, X. Mu, F. Zhang, and Y. Xu are with the Defense Key Disciplines Lab of Novel Micro-nano Devices and System Technology, International R&D center of Micro-nano Systems and New Materials Technology, Key Laboratory of Optoelectronic Technology & Systems, Ministry of Education, Chongqing University, Chongqing 400044, P. R. China.

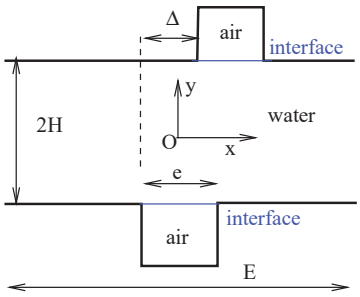

Fig. 1 Computation domain geometry

length than those employed on single wall, and it is not simply two times as perhaps expected due to the nonlinear interaction between the two walls [36]. This implies that the nonlinear interaction between the upper and lower channel walls would be modified (strengthened/weakened) by the phase shift of grooves on two walls, resulting in different drag reduction. However, it is difficult to align the micro-structures on the upper and lower channel walls due to the low assembling accuracy for the industrial applications, making it important to understand how this unalignment influences the performance of superhydrophobic microchannels. According to authors' best knowledge, there is few research work investigating how the phase shift of microstructures on the channel walls affects the slip length and thermal performance. Thus, this motivates the current work to study the effect of phase shift of transverse microgrooves of two walls on overall drag reduction, effective slip length in microchannels.

The numerical methodology is introduced in Section II, to be followed by the results on the effect of phase shift on slip length under different aspect ratio, Reynolds number and shear free fraction in Section III. Finally, the concluding remarks are given in Section IV.

II. Problem Formulation and Methodology

A. Problem Formulation and Governing Equations

As shown in Fig. 1 on the cross section of microchannel, the incompressible fluid (water) flows inside the channel bounded by the walls with gas (air) entrapped inside grooves. The flow is assumed to be laminar and steady, and the water-gas interface is assumed flat. The x-direction is the flow direction where a pressure gradient is applied to drive the flow, the y-direction is the direction of the channel height, and the origin is at the center of channel. The transverse grooves are arranged in a periodic array along the x-direction, therefore the flow is also periodic and two dimensional. As such, the computational domain can be simplified as two-dimensional, and the governing equations are given as follows:

$$\frac{\partial \rho u_i}{\partial x_i} = 0 \tag{1}$$

$$\frac{\partial \rho u_i u_j}{\partial x_i} = -\frac{\partial p}{\partial x_j} + \frac{\partial}{\partial x_i}\left(\mu \frac{\partial u_j}{\partial x_i}\right) \tag{2}$$

where p is the pressure.

Relative channel's aspect ratio

$$L = \frac{E}{D_h} = \frac{E}{4H},$$

Dimensionless shear free fraction

$$\delta = \frac{e}{E},$$

Dimensionless phase shift

$$\varepsilon = \frac{\Delta}{E},$$

where e is the shear-free region length, E is the module length, Δ is the shift length of the shear-free regions on the upper wall w.r.t. the lower wall, D_h is the channel's hydraulic diameter ($D_h \approx 4H$), and H is the half channel height.

Reynolds number

$$Re = \frac{\rho U_{avg} D_h}{\mu}$$

where the average bulk velocity $U_{avg} = \frac{\int_{-H}^{H} U dy}{2H}$, and

Periodic boundary conditions for the velocity are set at the inlet and outlet of the computational domain ($x = \pm E/2$): $u_{in} = u_{out}$; $v_{in} = v_{out}$; No-slip boundary condition is set in the solid region along the upper and lower walls ($y = \pm H$): $u = v = 0$, $T = T_w$; while shear-free boundary condition is set in the gas region $\partial u/\partial y = \partial v/\partial y = 0$.

Following the approach of other previous works [e.g. 26], the effective slip length λ is defined to characterize the friction reduction arising from the superdydrophobic surfaces by matching the flow resistance of the channel with slip boundary velocity as

$$u|_w = \lambda \left.\frac{\partial u}{\partial y}\right|_w.$$

The normalized effective slip length $\lambda/\delta e$ and the friction coefficient-Reynolds number product fRe are related via [26]

$$\frac{\lambda}{\delta e} = \frac{1}{L\delta^2}\left(\frac{8}{fRe} - \frac{1}{12}\right). \tag{3}$$

Note that $fRe = 96$ for the completely no-slip channel, thus the slip length becomes zero, which is consistent with (3). The Darcy friction factor f is defined as

$$f = \frac{\Delta P D_h}{\frac{1}{2}\rho U_m^2 E}.$$

where ΔP is the pressure loss, U_m is the bulk flow velocity $U_m = \frac{\int_{-H}^{H} U dy}{2H}$.

Note that the water-air interface is assumed flat under infinite surface tension in the current study, as most of previous computational studies did [28], [36], [33]. This idealized assumption makes the computations easier and helps to understand the mechanism of the phase shift effect without loss of generality.

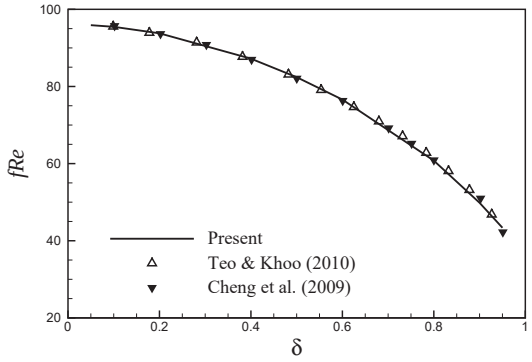

Fig. 2 Validation of numerical results in terms of friction coefficient fRe with different shear free fraction at $L = 1$ and $Re = 1$

B. Numerical Validation

Before the investigation propes, the accuracy of the assembled numerical code is tested vis-a-vis the smooth channels with slipless surface. In the specific implementation process, a staggered grid is used for the finite volume discretization, while the central difference scheme is employed for the spatial derivatives. The Crank-Nicolson scheme is applied for temporal discretization to advance solution from one time step to the next. The pressure field is updated by solving the Poisson equation to satisfy the continuity equation. This methodology and the code of flow solver has been employed and validated by the authors' previous publications [37]-[39].

For convenience of comparison, the product of friction coefficient f and Reynolds number Re (fRe) was used to validate the numerical code. As shown in Fig. 2, fRe approaches the analytical solution 96 when shear free fraction goes to zero and match well with the published results [40], [33]. It attests to the accuracy of the numerical code and is suitable for simulation of flow inside the superhydrophobic microchannel.

III. Results and Discussion

In this section, the effect of phase shift ε between upper and lower super-hydrophobic sections on the effective slip length $\lambda/\delta e$ is studied and discussed. Generally, the nondimensional effective slip length $\lambda/\delta e$ depends on the channel's aspect ratio L, shear free fraction δ, and the working condition like Reynolds number Re. Thus, the modulation effect of phase shift ε on the frictional and thermal performance can be expected. So, the variation of slip length $\lambda/\delta e$ due to phase shift ε are investigated at different aspect ratio L, Reynolds number Re and shear free fraction δ as shown in Table I. Note that the parameters set in *Italic* (at $L = 2$, $Re = 1$, and $\delta = 0.5$) are chosen the reference case to show how these parameters affect the performance of the microchannel with different phase shift. The friction reduction capability is investigated in terms of nondimensional slip length $\lambda/\delta e$.

A. Aspect Ratio

The aspect ratio L dramatically influences the overall friction coefficient of microchannels, and hence affects the slip length $\lambda/\delta e$ (Teo & Khoo, Cheng et al. 2012). So, it is logical to study how the phase shift modulate the slip length at different aspect ratios.

TABLE I
Parameters of Investigated Microchannels at Different Phase Shift $\varepsilon = 0$, 0.1, 0.2, 0.3, 0.4 and 0.5

Parameters	
aspect ratio L	0.25, 0.5, 0.8, 1, 1.25, 1.6, *2*, 2.5
shear free fraction δ	0.05, 0.1, 0.2, 0.4, *0.5*, 0.6, 0.8, 0.9, 0.95
Reynolds number Re	*1*, 2, 5, 10, 20, 50, 100, 200, 500, 1000

Fig. 3 demonstrates the variation of slip length $\lambda/\delta e$ due to phase shift at different aspect ratio from 0.25 to 2.5. Herein, a typical shear free fraction $\delta = 0.5$ is chosen and both low and high Reynolds numbers at $Re = 1$, 1000 are studied for simplicity without loss of generality. It can be seen from Fig. 3 that the effective slip length $\lambda/\delta e$ increases with phase shift ε at the same aspect ratio. In addition, the variation of the effective slip length $\lambda/\delta e$ due to the phase shift ε becomes greater at high aspect ratio. Similarly, comparison of the results at the two different Reynolds numbers $Re = 1$ and 1000 demonstrates that phase shift has much more obvious effect on slip length at relatively low Reynolds number ($Re = 1$), which is also the most pertinent working conditions for microchannel flows. It is observed that the effective slip length $\lambda/\delta e$ with zero phase shift decreases with the aspect ratio L for both low and high Reynolds numbers. However, the effective slip length is dramatically increased by shifting ε at low Reynolds number ($Re = 1$) and high aspect ratio (see Fig. 3(a)). Such changes in slip length due to phase shift (difference between $\varepsilon = 0$ and 0.5) gradually increases within $L = 0.25$–1.2 and then almost remains as an constant for $L = 1.2$–2.5. So the highest slip length is achieved at $L = 1.2$ and $\varepsilon = 0.5$ for $Re = 1$, where the increase of slip length due to the change in phase shift overcomes the decrease of slip length due to the increase of aspect ratio. Thus, an interesting phenomenon found is that $\lambda/\delta e$ increases then decreases with aspect ratio L at high enough phase shift ($\varepsilon > 0.3$). Conversely, the original decreasing trend of slip length against the aspect ratio for the reference case (with $\varepsilon = 0$) is maintained at high Reynolds number ($Re = 1000$, see Fig. 3(b)) with nonzero phase shift.

B. Reynolds Number

Though microchannels are normally operating at relatively small Reynolds number ($Re < 1$), it is still worthwhile to investigate the effect of phase shift on the slip length at different Reynolds numbers ranging from $Re = 1$ to 1000.

Fig. 4 demonstrates the variation of the effective slip length $\lambda/\delta e$ due to phase shift ε at different Reynolds number for aspect ratio $L = 0.25$, 2 and a typical shear free fraction at $\delta = 0.5$. It is shown that the effect of phase shift on slip length is quite negligible at all Reynolds numbers ranging from 1 to 1000 for small aspect ratio ($L = 0.25$, see Fig. 4(a)). It is also observed that the slip length $\lambda/\delta e$ is significantly increased by shifting the shear free section for high aspect ratio ($L = 2$, see Fig. 4(b)). Such increase of slip length is more obvious at relatively low Reynolds number ($Re = 1$–10), and gradually

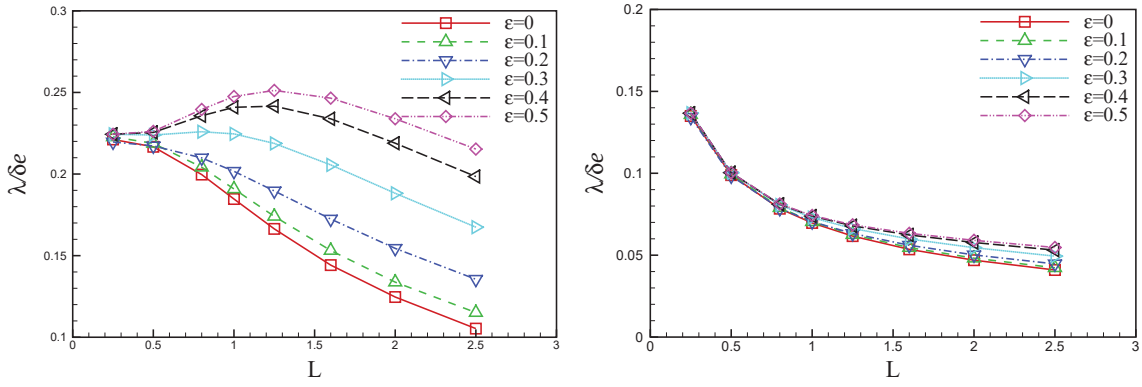

(a) $Re = 1$ (b) $Re = 1000$

Fig. 3 Variation of the slip length $\lambda/\delta e$ due to phase shift ε at different aspect ratio L for $Re = 1$, 1000 and $\delta = 0.5$

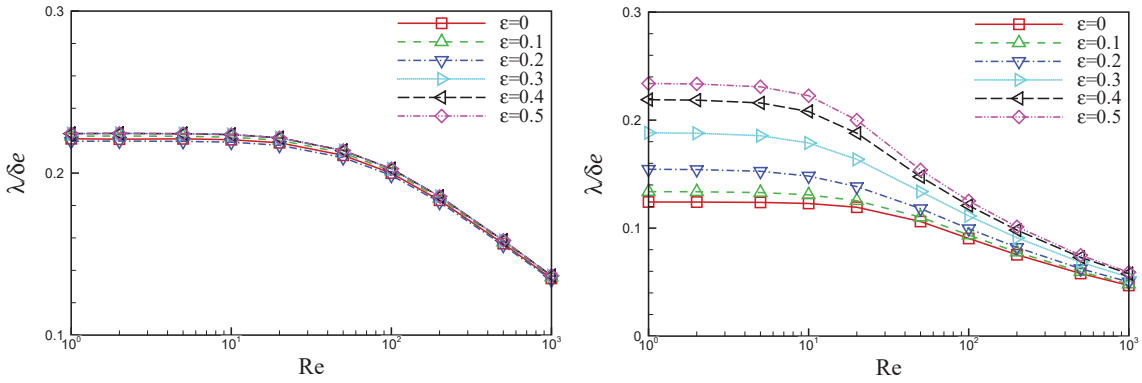

(a) $L = 0.25$ (b) $L = 2$

Fig. 4 Reynolds number effect on the slip length λ $\lambda/\delta e$ at $L = 0.25$, 2 and $\delta = 0.5$

drops to a low level while Reynolds number increases up to 1000.

Combining with the findings in the previous section, it can be concluded that the phase shift increases the slip length more significantly at high aspect ratio (L = 1–2.5) and low Reynolds number Re = 1–10.

C. Shear Free Fraction

Besides the aspect ratio and Reynolds number, the effect of phase shift on slip length at different shear free fraction is investigated and presented in Fig. 5.

As perhaps expected, the variation of slip length due to the phase shift is extremely small at low aspect ratio or high Reynolds number (see Figs. 5(a), (c) and (d)), while the variation of slip length is significant only when the aspect ratio is high and Reynolds number is low (see Fig. 5(b)). The increases of slip length induced by phase shift at different shear free fraction are of the same order for $L = 2$ and $Re = 1$ with wide shear free fraction ranging in the interval $0.3 < \delta < 0.95$ (see Fig. 5(b)), thus the trend of slip length against the shear free fraction is broadly unchanged by the phase shift although the higher shear free free fraction induces greater slip length.

D. Summary

From the above discussions on the variation of slip length due to phase shift at different aspect ratio, Reynolds number and shear free fraction, it is found that the phase shift significantly increases the slip length at relatively high aspect ratio ($L > 1$) and low Reynolds number ($Re < 10$) for very wide shear free fraction range ($0.3 < \delta < 0.9$).

IV. Conclusion

In this paper, a numerical study on the flow inside microchannel with superhydrophobic walls with rib-groove structures was conduced based on the developed CFD tool, to study the effect of phase shift of grooves between the upper and lower walls. The numerical results showed that the shifted grooves on the upper and lower walls can increase the effective slip length by up to 100% especially for the high aspect ratio ($L = 2$), low Reynolds number ($Re = 1$) within a wide shear free fraction range (δ = 0.05–0.95). In conclusion, shifting the transverse grooves on the upper and lower walls of superhydrophobic microchannel can further increase the slip length (reduce the friction). In the future, the experimental investigation is required to further confirm the accuracy and feasibility of the numerical findings in this study. The curvature of the air-water interface including its surface tension effect also

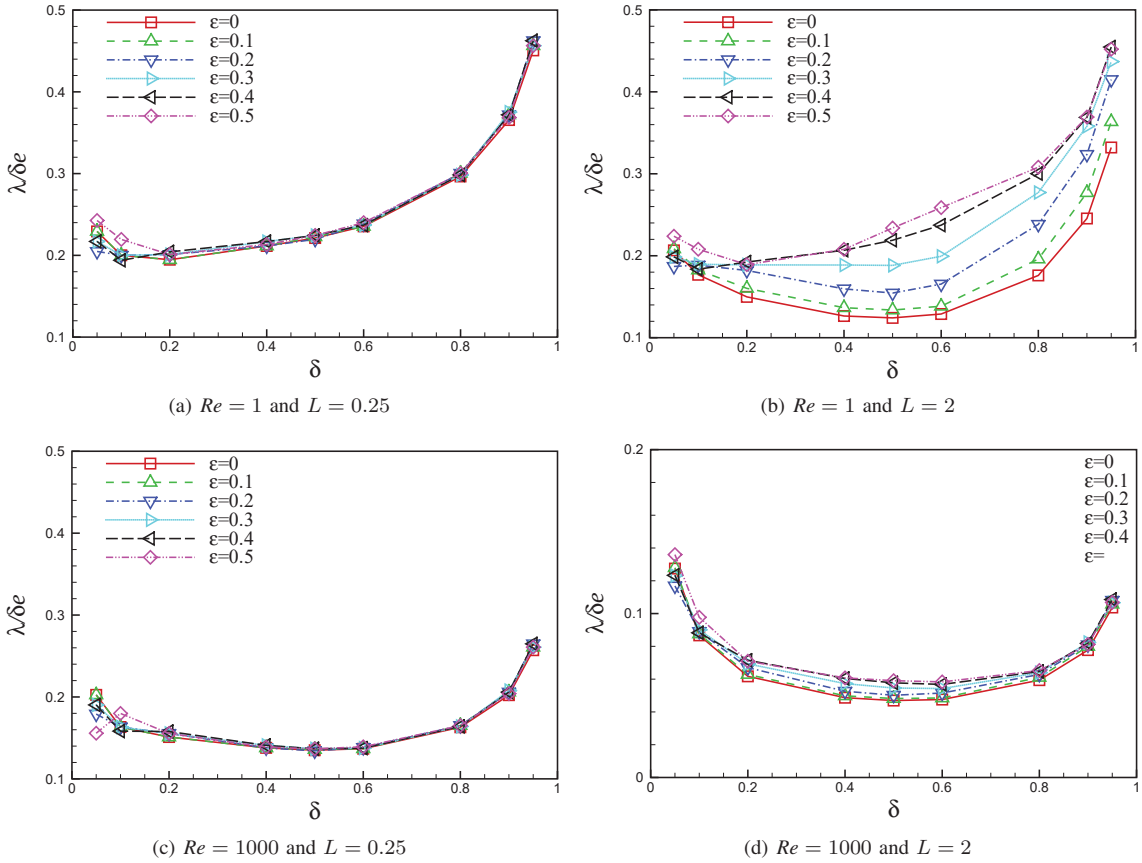

(a) $Re = 1$ and $L = 0.25$ (b) $Re = 1$ and $L = 2$

(c) $Re = 1000$ and $L = 0.25$ (d) $Re = 1000$ and $L = 2$

Fig. 5 The effect of the fraction of slip space δ on the slip length $\lambda/\delta e$ at $Re = 1$, 1000 and $L = 0.25$, 2

needs to explored. Besides, superhydrophobic microchannel with non-aligned/shifted longitudinal grooves shall also be investigated similar to the transverse grooves herein.

Acknowledgment

This project is supported by core funding of IHPC (A*STAR), National Key Research and Development Program of China (Grant No.2016YFB0402702), National Natural Science Foundation of China (Grant No. 51605060), the Fundamental Research Funds for the Central Universities (No.106112016CDJZR125504), Ministry of Education of the People's Republic of China, Joint Foundation of Equipment Pre-Research and the Ministry of Education of China(Grant No.6141A02033402), and the "thousands talents" program for the pioneer researcher and his innovation team, China.

Disclaimer

The views expressed in this paper are those of the authors and do not necessarily reflect those of their affiliated companies.

References

[1] H. A. Stone, A. D. Stroock, A. Ajdari, Engineering flows in small devices: microfluidics toward a lab-on-a-chip, Annu. Rev. Fluid Mech. 36 (2004) 381–411.
[2] G. Hagen, Uber den Einfluss der Temperatur auf die Bewegung des Wasser in Röhren, Math. Abh. Akad. Wiss. 17.
[3] H. Darcy, Recherches expérimentales relatives au mouvement de l'eau dans les tuyaux, Mallet-Bachelier, 1857.
[4] J. Nikuradse, Strömungsgesetze in Rauhen Rohren, VDI-Forschungscheft 361; also NACA TM 1292 (1950) .
[5] L. F. Moody, N. J. Princeton, Friction factors for pipe flow, Trans. ASME 66 (8) (1944) 671–684.
[6] R. García-Mayoral, J. Jiménez, Drag reduction by riblets, Philosophical Transactions of the Royal Society of London A: Mathematical, Physical and Engineering Sciences 369 (1940) (2011) 1412–1427.
[7] J. P. Rothstein, Slip on superhydrophobic surfaces, Annual Review of Fluid Mechanics 42 (2010) 89–109.
[8] W. Barthlott, C. Neinhuis, Purity of the sacred lotus, or escape from contamination in biological surfaces, Planta 202 (1) (1997) 1–8.
[9] C. Navier, Mémoire sur les lois du mouvement des fluides, Mémoires de L'Académie Royale de Sciences de L'Institut de France 6 (1823) 389–440.
[10] J. C. Maxwell, On stresses in rarified gases arising from inequalities of temperature, Philosophical Transactions of the royal society of London 170 (1879) 231–256.
[11] J. Ou, B. Perot, J. P. Rothstein, Laminar drag reduction in microchannels using ultrahydrophobic surfaces, Physics of Fluids 16 (12) (2004) 4635–4643.
[12] B. Woolford, K. Jeffs, D. Maynes, B. Webb, Laminar fully-developed flow in a microchannel with patterned ultrahydrophobic walls, in: ASME 2005 Summer Heat Transfer Conference collocated with the ASME 2005 Pacific Rim Technical Conference and Exhibition on Integration and Packaging of MEMS, NEMS, and Electronic Systems, American Society of Mechanical Engineers, 481–488, 2005.
[13] O. I. Vinogradova, Slippage of water over hydrophobic surfaces, International journal of mineral processing 56 (1) (1999) 31–60.
[14] G. E. Karniadakis, A. Beskok, N. Aluru, Microflows and nanoflows: fundamentals and simulation, vol. 29, Springer Science & Business Media, 2006.
[15] E. Lauga, M. Brenner, H. Stone, Microfluidics: the no-slip boundary condition, in: Springer handbook of experimental fluid mechanics,

Springer, 1219–1240, 2007.
[16] X. Zhang, F. Shi, J. Niu, Y. G. Jiang, Z. Q. Wang, Superhydrophobic surfaces: from structural control to functional application, Journal of Materials Chemistry 18 (6) (2008) 621–633.
[17] M. Zhou, J. Li, C. X. Wu, X. K. Zhou, L. Cai, Fluid drag reduction on superhydrophobic surfaces coated with carbon nanotube forests (CNTs), Soft Matter 7 (9) (2011) 4391–4396.
[18] L. C. Gao, T. J. McCarthy, A perfectly hydrophobic surface (θA/θR= 180/180), Journal of the American Chemical Society 128 (28) (2006) 9052–9053.
[19] D. Quéré, Wetting and roughness, Annu. Rev. Mater. Res. 38 (2008) 71–99.
[20] M. Reyssat, J. M. Yeomans, D. Quéré, Impalement of fakir drops, Europhys. Lett. 81 (2008) 26006.
[21] M. A. Samaha, H. V. Tafreshi, M. Gad-el Hak, Modeling drag reduction and meniscus stability of superhydrophobic surfaces comprised of random roughness, Physics of Fluids 23 (1) (2011) 012001.
[22] E. Lauga, H. A. Stone, Effective slip in pressure-driven Stokes flow, Journal of Fluid Mechanics 489 (2003) 55–77.
[23] C.-H. Choi, C.-J. Kim, Large slip of aqueous liquid flow over a nanoengineered superhydrophobic surface, Physical Review Letters 96 (6) (2006) 066001.
[24] C. Lee, C.-H. Choi, et al., Structured surfaces for a giant liquid slip, Physical review letters 101 (6) (2008) 064501.
[25] C. Ybert, C. Barentin, C. Cottin-Bizonne, P. Joseph, L. Bocquet, Achieving large slip with superhydrophobic surfaces: Scaling laws for generic geometries, Physics of Fluids (1994-present) 19 (12) (2007) 123601.
[26] J. Davies, D. Maynes, B. W. Webb, B. Woolford, Laminar flow in a microchannel with superhydrophobic walls exhibiting transverse ribs, Physics of Fluids 18 (8) (2006) 87110.
[27] S. Gogte, P. Vorobieff, R. Truesdell, A. Mammoli, F. van Swol, P. Shah, C. J. Brinker, Effective slip on textured superhydrophobic surfaces, Physics of fluids 17 (5) (2005) 51701–51701.
[28] Y. P. Cheng, C. J. Teo, B. C. Khoo, Microchannel flows with superhydrophobic surfaces: Effects of Reynolds number and pattern width to channel height ratio, Physics of Fluids 21 (2009) (2009) 1–12.
[29] A. Steinberger, C. Cottin-Bizonne, P. Kleimann, E. Charlaix, High friction on a bubble mattress, Nature materials 6 (9) (2007) 665–668.
[30] A. M. Davis, E. Lauga, Geometric transition in friction for flow over a bubble mattress, Physics of Fluids (1994-present) 21 (1) (2009) 011701.
[31] C.-O. Ng, C. Wang, Stokes shear flow over a grating: implications for superhydrophobic slip, Physics of Fluids (1994-present) 21 (1) (2009) 013602.
[32] J. Hyväluoma, J. Harting, Slip flow over structured surfaces with entrapped microbubbles, Physical review letters 100 (24) (2008) 246001.
[33] C. J. Teo, B. C. Khoo, Flow past superhydrophobic surfaces containing longitudinal grooves: Effects of interface curvature, Microfluidics and Nanofluidics 9 (2-3) (2010) 499–511.
[34] C. J. Teo, B. C. Khoo, Effects of interface curvature on Poiseuille flow through microchannels and microtubes containing superhydrophobic surfaces with transverse grooves and ribs, Microfluidics and Nanofluidics 17 (5) (2014) 891–905.
[35] N. Kashaninejad, N.-T. Nguyen, W. K. Chan, Eccentricity effects of microhole arrays on drag reduction efficiency of microchannels with a hydrophobic wall, Physics of Fluids 24 (11) (2012) 112004.
[36] C. J. Teo, B. C. Khoo, Analysis of Stokes flow in microchannels with superhydrophobic surfaces containing a periodic array of micro-grooves, Microfluidics and Nanofluidics 7 (3) (2009) 353–382.
[37] W. Ren, C. Shu, J. Wu, W. Yang, Boundary condition-enforced immersed boundary method for thermal flow problems with Dirichlet temperature condition and its applications, Computers & Fluids 57 (2012) 40–51.
[38] W. Ren, J. Wu, C. Shu, W. Yang, A stream function–vorticity formulation-based immersed boundary method and its applications, International Journal for Numerical Methods in Fluids 70 (5) (2012) 627–645.
[39] C. Shu, W. Ren, W. Yang, Novel immersed boundary methods for thermal flow problems, International Journal of Numerical Methods for Heat & Fluid Flow 23 (1) (2013) 124–142.
[40] Y. Cheng, J. Xu, Y. Sui, Numerical study on drag reduction and heat transfer enhancement in microchannels with superhydrophobic surfaces for electronic cooling, Applied Thermal Engineering (2014) 1–11.